IEEE Access
Multidisciplinary | Rapid Review | Open Access Journal

Received August 25, 2021, accepted September 8, 2021, date of publication September 20, 2021,
date of current version September 28, 2021.

Digital Object Identifier 10.1109/ACCESS.2021.3113899

Transparent Wideband Circularly Polarized GNSS Antenna for Vehicular Applications

ALIREZA GHARAATI, (Graduate Student Member, IEEE), MOHAMMAD SAEID GHAFFARIAN, (Member, IEEE), AND RASHID MIRZAVAND, (Senior Member, IEEE)
Intelligent Wireless Technology Laboratory, University of Alberta, Edmonton, AB T6G 1H9, Canada

Corresponding author: Rashid Mirzavand (mirzavan@ualberta.ca)

This work was supported in part by the Natural Sciences and Engineering Research Council of Canada (NSERC) and in part by Alberta Innovate (AI).

ABSTRACT In this paper, a single-layer one-sided wideband coplanar waveguide (CPW)-fed transparent circularly polarized (CP) rectangular slot antenna with tilted beam is proposed. The antenna is designed on a glass substrate with a mesh grid in the conductive layer in order to increase the transparency. Since most of the vehicles' windshields are inclined for about 30 degrees, the beam of the antenna is designed to be tilted for about 30 degrees in elevation. For measurement verification, an inclined stage is fabricated to resemble the inclined surfaces (such as the windshields). The 10-dB impedance bandwidth of the antenna is 40.8% (1.13 - 1.71 GHz) with a 3-dB axial ratio bandwidth of 47.4% (1.06 - 1.72 GHz) and a 3-dB gain bandwidth of about 54% (1.02 - 1.78 GHz) with a maximum right handed circular polarization (RHCP) gain of 5.3 dBic. Also, the transparency of the antenna is about 95%. Therefore, the antenna is a good candidate for vehicular applications such as location tracking, using global navigation satellite system (GNSS) and specifically global positioning systems (GPS). Furthermore, a small-size transparent reflector is designed to be used below the proposed antenna in order to increase the front to back ratio (FBR).

INDEX TERMS Characteristic mode analysis (CMA), circularly polarized (CP) antenna, global navigation satellite system (GNSS), global positioning systems (GPS), slot antenna, tilted beam, transparent antenna, vehicular applications.

I. INTRODUCTION

The advancement of circularly polarized (CP) antennas in wireless communication systems in the past years have been significant and impressive [1]. They have several advantages over the linearly polarized (LP) ones, such as reduction of multipath interference and fading effects and prevention of polarization mismatch due to Faraday rotation effects [2].

CP antennas are used widely in many applications. One of the most important applications of CP antennas are in global navigation satellite systems (GNSS), designed and developed for positioning and time data transfer, starting from 1164 MHz to 1610 MHz. The global positioning system (GPS) is one of such systems in which CP antennas play important role. The GPS has been used widely in many applications such as military and civilian fields, location tracking, and so on [3], [4]. For GPS applications, the antenna should radiate a right hand circular polarization (RHCP) wave and desired to have a high front to back ratio (FBR). To cover the whole GNSS bands, wideband CP antennas are needed. Many of such antennas have been proposed recently [5]–[7].

Most of antennas designed for GPS applications have a maximum beam at boresight because of line-of-sight (LoS) environments. However, by mounting the antenna on an inclined surface, the maximum beam does not occur at zenith anymore. Hence, a tilted beam antenna with a tilted angle equal to the inclination angle of the surface is needed in order to see the sky for the LoS applications. In recent years, different types of antennas with tilted beam and several techniques for steering the beam have been introduced, among them are four arm spiral antennas with beamforming circuit antennas [8], asymmetric bow-tie antenna [9], dielectric

The associate editor coordinating the review of this manuscript and approving it for publication was Zhenhui Yuan.

resonator antenna [10], and many others. To place an antenna on inclined surfaces, like a windshield of a vehicle, having a tilted beam is necessary due to the fact that for location tracking applications in GPS systems, the beam of the antenna should see the sky for a better performance. However, by putting the antenna on the windshield, the vision of the driver might get blocked. Hence, it necessitates the presence of a transparent antenna.

Researchers are paying more attention and interest in transparent devices, especially for wireless communication applications. Transparent antennas are being used in many applications nowadays [11]. Different types of materials are used in transparent devices. Conductive oxides are such materials used vastly in transparent electronic devices as they represent a high optical transparency (OT), such as indium tin oxide (ITO) and fluorine doped tin oxide (FTO) [12]. The problems of these transparent materials, however, are their cost, high surface resistance, and scarcity [13]. Another method used for transparent antennas is the usage of metal mesh grid, which has high conductivity and low resistance compared to transparent conductive oxides [12], [14]. As a result, mesh grid method is more preferred and investigated in recent years [15], [16].

In this paper, a single-layer coplanar waveguide (CPW)-fed wideband circularly polarized transparent antenna with tilted beam is proposed. No other such antennas were introduced to have the above-mentioned characteristics simultaneously in the literature. The antenna is designed and can be used for any inclined surfaces which need LoS applications. Here, the proposed antenna is designed especially for GPS location tracking for vehicular platforms. Since most windshields are inclined for around 30 degrees in elevation, the beam of the antenna is also designed for a tilt of about 30 degrees. In this case, the maximum RHCP gain, which is vital for GPS applications, occurs at zenith when it is mounted on the windshield. Furthermore, to increase the FBR, a transparent reflector is designed and fabricated in order to be placed inside the car, on the dashboard or glove compartment of the vehicle. The antenna exhibits a wide 10-dB impedance bandwidth and also a wide 3-dB axial ratio bandwidth covering all GNSS frequencies. Moreover, the 3-dB gain bandwidth of the antenna shows a stable bandwidth throughout the desired frequency band. Obtaining all the characteristics together in a single-layer antenna is the main goal of this work. To analyze the operation mechanism of the proposed antenna, characteristic mode analysis (CMA) is performed, which has been an interesting and attractive analysis among the researchers in recent years.

The rest of the paper is organized as follows. Section II introduces the configuration of the antenna and development stages. In section III, the CMA is carried out in details. Section IV talks about the antenna analysis and introduction of transparent reflector. The fabrication process and discussions of results are represented in Section V. Finally, the paper is concluded in Section VI.

II. CONFIGURATION AND DEVELOPMENT OF THE PROPOSED ANTENNA

A. ANTENNA GEOMETRY

The configuration of the proposed antenna is shown in Fig. 1. The single-layer single-sided antenna is designed on a transparent glass substrate with a relative permittivity of $\epsilon_r = 5.5$ and a thickness of 1mm, with dimensions of 149×99 mm^2. The CPW line is fed by a coaxial feedline with an input impedance of 50 Ω. The exact dimensions of different sections are shown in Fig. 2. Another key point to remember is the fact that since the antenna is intended to be transparent, a mesh grid is used throughout the antenna instead of full conductive layer. Most of the mesh grid elements consist of square elements with a length of 5.4 mm and a width of 0.1 mm (see Fig. 2 (d)). In some minor areas, however, the size of mesh elements are modified relative to the constraints in terms of space. For calculating the transparency, the general equation for a periodic mesh grid surface with

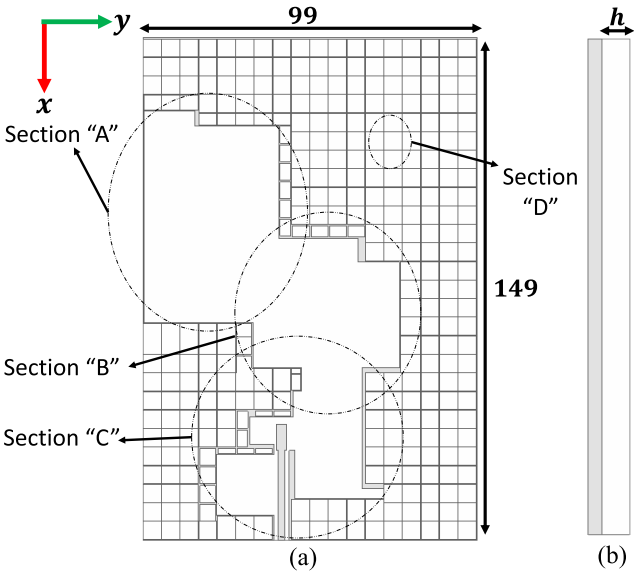

FIGURE 1. Geometry of the proposed antenna, (a) top view (b) side view. $h = 1$ (dimensions in mm).

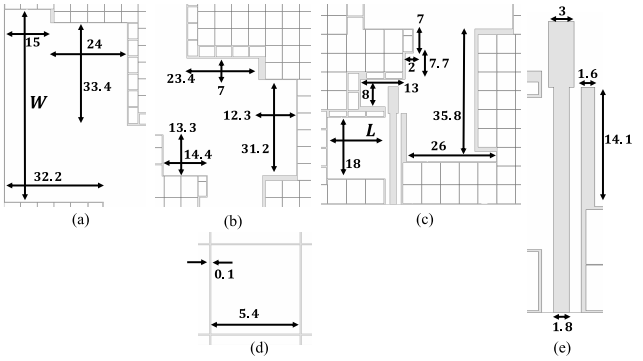

FIGURE 2. Enlarged sections of the proposed antenna, (a) section A (b) section B (c) section C (d) section D (e) enlarged section of feedline. $W = 63$, $L = 17$ (all dimensions are in mm).

equal sized elements is defined as follows:

$$OT = (\frac{m}{m+n})^2 \quad (1)$$

where 'm' is the length and 'n' is the width of mesh element (for the proposed antenna are 5.4 and 0.1 mm, respectively). For a surface having mesh elements with different sizes, the transparency is obtained by the ratio of the whole and open areas. In this case, the transparency of the antenna is calculated for about 95 %. Furthermore, a new coordinate system is defined in which most of the simulation and measurement results are performed. The new coordinate system in which the antenna is mounted on the windshield of a car is illustrated in Fig. 3.

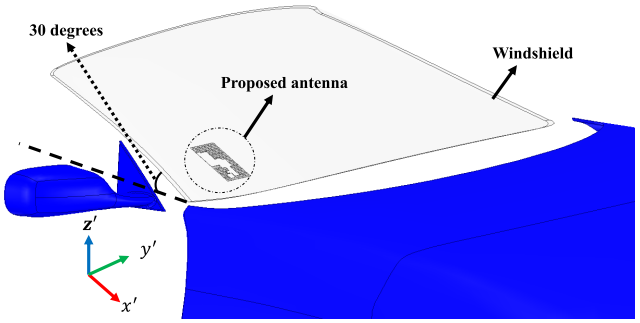

FIGURE 3. Definition of the new coordinate system while the antenna is placed on the windshield.

B. ANTENNA DEVELOPMENT STAGES

Five different stages of the antenna evolution are depicted in Fig. 4. Since the desired antenna should have a tilted beam, an asymmetric rectangular slot is etched on the conductive layer being fed by a CPW feedline not in the middle (see Fig. 4 (a)). This will result in a tilted beam in the desired frequency band since the surface current distribution is asymmetric, and causing two resonance frequencies near 1.35 GHz and 1.75 GHz. The reflection coefficient and axial ratio of all antennas are shown in Fig. 5, obtained in the new coordinate system. Also, the magnitude ratio of two orthogonal field components of E_x and E_y are demonstrated in Fig. 6. To reach CP, from the theory, the magnitude ratio of E_x and E_y should reach 1 with a 90° phase difference. However, since the magnitude ratio of two orthogonal field components of E_x and E_y is high, Ant1 does not radiate a CP wave. In order to overcome this problem, three rectangular strips are added at three different corners of the rectangular slot. This will cause the magnitude ratio of E_x and E_y to drop for a significant value, but still an inappropriate phase difference (PD) between E_x and E_y remains which does not form circular polarization. Therefore, in this step, another strip is added at the middle and the size of the slot is reduced in the right section and increased in the bottom section, forming Ant3 (see Fig. 4 (c)). Hence, the magnitude ratio and phase difference of E_x and E_y are changed to the appropriate values, causing axial ratio below 3-dB for the desired bandwidth. To improve the impedance

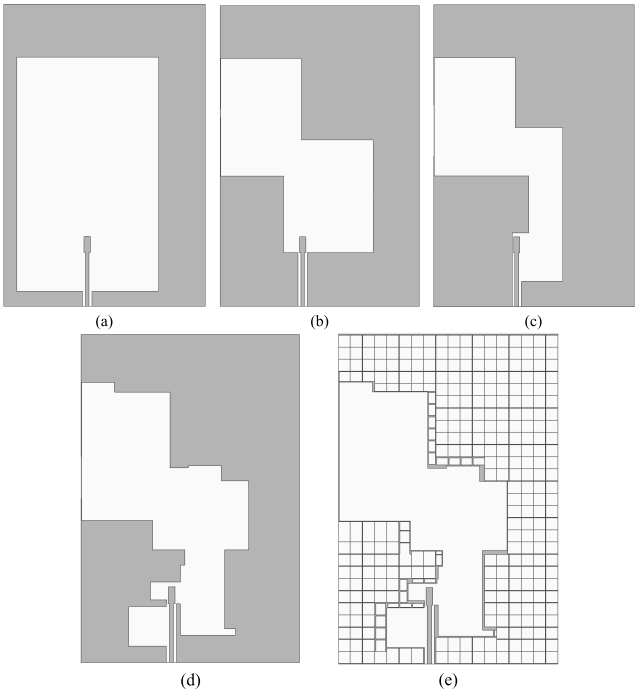

FIGURE 4. Antenna evolution stages, (a) Ant1 (b) Ant2 (c) Ant3 (d) Ant4 (e) proposed antenna.

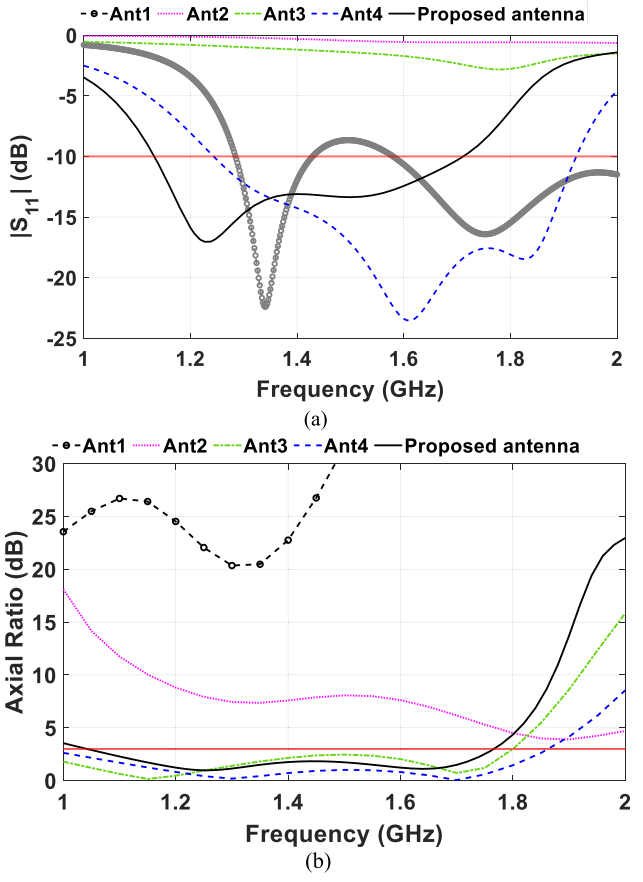

FIGURE 5. Reflection coefficient and axial ratio of Ant1-Ant4 and the proposed antenna, (a) reflection coefficient (b) axial ratio at $\theta' = 0, \phi = 0$.

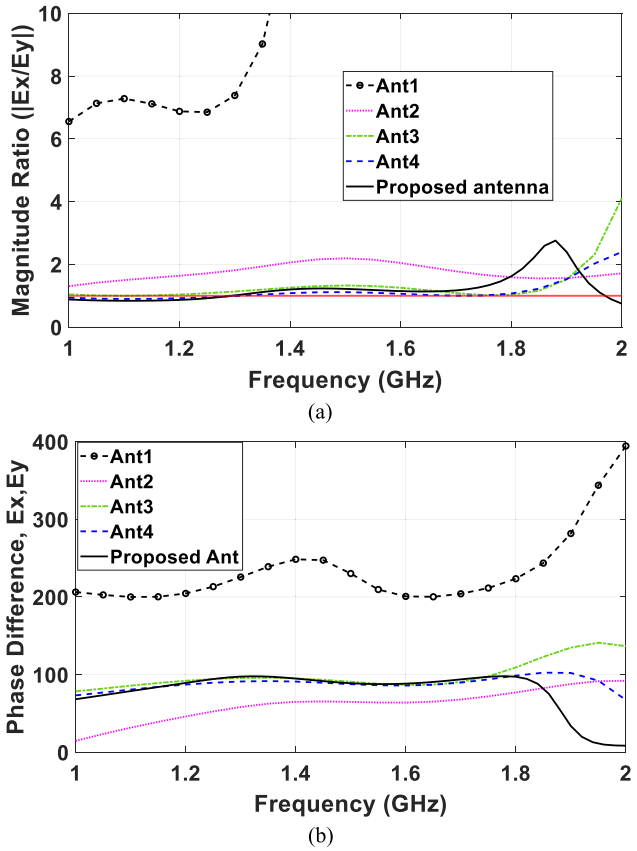

FIGURE 6. Magnitude ratio and phase difference (PD) of orthogonal field components E_x and E_y, (a) magnitude ratio, (b) phase difference (PD unit is in degree).

bandwidth, several small-size slots are added to different parts of the antenna, as can be seen in Fig. 4 (d), forming Ant4. Finally, mesh grid is applied to the antenna to make the antenna transparent. It is worth mentioning that the axial ratio of different antennas are depicted in the new coordinate system.

III. CHARACTERISTIC MODE ANALYSIS

Characteristic modes (CMs) are natural inherent modes of a structure, independent of the geometry and feeding of the design. The idea of characteristic mode analysis was initially introduced in [17] by Garbacz and Turpin, and enhanced by Harrington and Mautz [18]. In recent years, CMA has been very popular among researchers, since it is a powerful tool among researchers and engineers for designing antennas. As a physical interpretation, the CMs are a set of orthogonal modes for expanding any induced currents on a perfect electric conductor (PEC) material, which can be defined as following [19]:

$$J_{total} = \sum_{n=1}^{N} a_n J_n \tag{2}$$

where a_n are the complex modal expansion coefficients for each mode, and J_n are the characteristic currents. The normalized amplitude of the characteristic currents is called modal significance (MS) which can be shown as:

$$MS_n = |\frac{1}{1+j\lambda_n}| \tag{3}$$

obtained by solving the generalized eigenvalue problem:

$$Z = R + jX \tag{4}$$

$$XJ_n = \lambda_n RJ_n \tag{5}$$

where λ_n are the eigenvalues, 'R' and 'X' are Hermitian real and imaginary parts of the impedance matrix Z, respectively. Also, characteristic angle (CA) which represents the phase angle between a characteristic current and the associated characteristic field is defined as:

$$CA = 180^\circ - \arctan(\lambda_n) \tag{6}$$

A resonance occurs when the eigenvalue is equal to zero ($MS = 1$ or $CA = 180^\circ$). For having a circular polarization, two orthogonal modes should be excited simultaneously with a 90° phase difference. These modes should have the following requirements [20]–[23]:

1) The MS values should almost be the same.
2) The CAs should have about a 90° phase delay.
3) The directivities should be the same at the desired angle.
4) The current distribution of the two modes should be orthogonal.

There are some key factors which should be considered in the analysis. First, to adjust the impedance bandwidth, modes with appropriate modal significance values should be found at the desired frequencies. Then, to produce the circular polarization, pairs of modes having appropriate modal significance values with the same directivities at the desired angle should be found. These pairs also should have a 90 degrees phase delay in their CAs to create perfect circular polarization. That being said, a phase delay close to 90 degrees can also contribute to circular polarization (AR<3dB). Noteworthy, the surface currents of pair modes should be orthogonal in this case. To reach the desired goal of designing a CP antenna with tilted beam in the desired frequency bands, CMA is performed for every stage. In fact, by using CMA step by step, the performance of the antenna gets better and closer to the end goal, either by improving the impedance or the axial ratio bandwidths. This is applicable by observing the behaviour of each mode and comparing them to each other. Moreover, by plotting the surface currents for each mode (or pair modes) at specific frequencies, it can be inferred which area of the antenna to be altered. For example, the surface currents for two orthogonal modes can depict the areas where some changes in the structure of the antenna can cause a change in the value of the MS or the CA, specifically showing that by making changes in the two main slots, significant improvements could be achieved. Hence, it can give some hints how to update each step. In other words, the CMA is a guideline for reaching the next step.

With this in mind, CMA is first performed for Ant2. By observing the most effective modes in the desired bandwidth (first six modes), the resonances can be found where $MS = 1$ (or $CA = 180°$). That implies the potential modes and frequencies where resonance can occur. By plotting the surface currents of a mode (or pair modes) at a specific frequency, it can be inferred which area to change in order to have the most effects on the modes. This could be inferred either by the magnitude or the phase of the surface current. Although the results might show a potential mode causing a wide impedance bandwidth, the antenna might not be matched to a 50 Ω input. In this case, as said earlier, some regions with the most effects on that specific mode needs to be altered.

For reaching circular polarization, different approaches can be taken into consideration. One approach is to find the intersection of each pair modes (where the MS of that pair mode is equal) and observe the CA difference, directivities, and surface currents of that two modes. In this approach, the surface currents can help finding the regions with most effects on the circular polarization, and consequently, altering those regions in a way that the pair modes be able to make circular polarization. The MS and CA of Ant2 is shown in Fig. 7 (a) and (b). As an example of the above-mentioned approach, the intersection of mode 2 and mode 4 at 1.75 GHz is chosen for investigation. Both modes have the same MS values at this frequency, with CA difference of 64 degrees. Also, the far-field radiation pattern of each mode shows almost the same directivities in the desired angle. However, the surface currents are not orthogonal (shown with black arrows). Therefore, although it is not CP at this frequency, it has the potential to become. As shown in Fig. 7 (c), there are some regions highlighted with red dash lines where the magnitudes of surface currents are higher than other regions. This can give a clue where to change, especially the regions which are common between mode 2 and mode 4 (the two regions at the bottom of the structure, enclosed with red dash line). Making changes in these two regions leads to Ant3. This approach can be extended for every pair modes in any antennas, from Ant2 to Ant4, where a potential CP can be made (for each step, the four requirements should be checked out).

As another approach, specific frequencies can be chosen for each antenna (1.227 GHz as an example). Again, by plotting MSs, CAs, directivities, and surface currents at 1.227 GHz, a pair of modes which are capable of producing circular polarization can be chosen. Then, by plotting the surface currents, alterations should be made in a way that the pair modes get close to circular polarization (same as previous approach).

After taking all these steps and applying the alterations in the structure of the antennas, the proposed antenna is reached. To make it short and concise, only the final results of the proposed antenna are displayed, except for the surface currents which is for Ant4, since the results of Ant4 and the proposed antenna are almost the same and the only difference of these

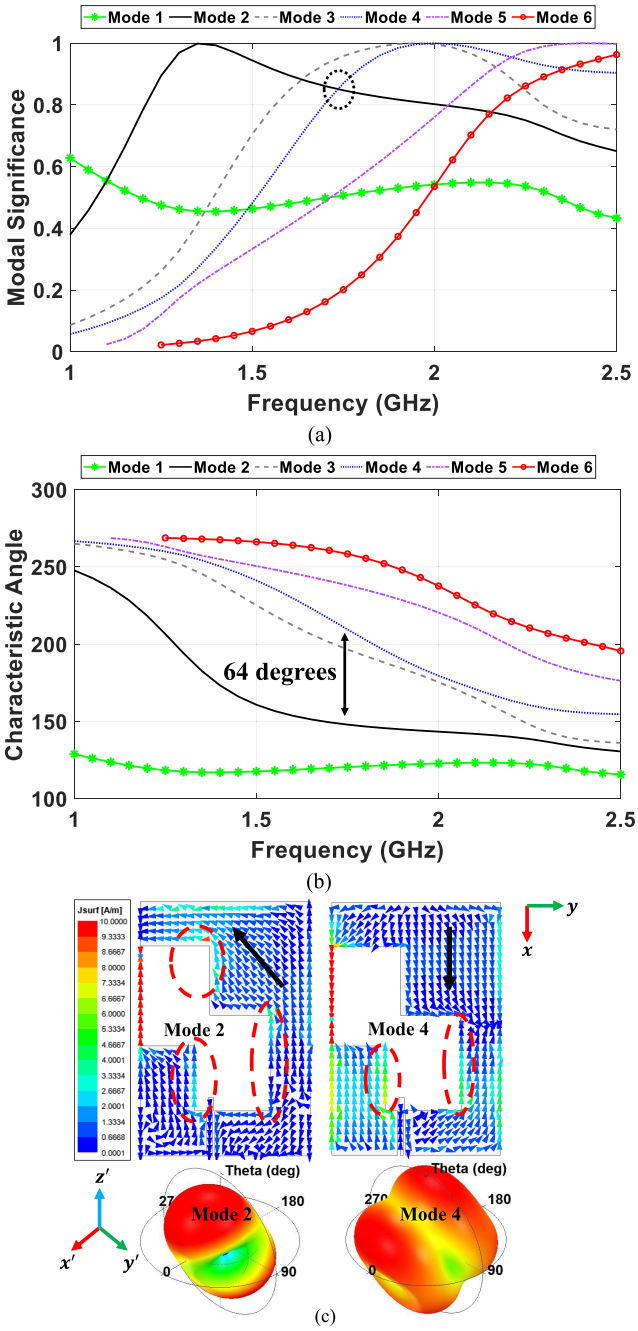

FIGURE 7. Characteristic mode analysis of Ant2 (a) modal significance (b) characteristic angle (c) surface currents and directivities of modes 2 and 4 at 1.75 GHz.

two antennas are in terms of their transparency, where Ant4 is turned into the proposed antenna by applying mesh grid throughout the design, making it transparent. The MS and CA of the proposed antenna are illustrated in Fig. 8 (a) and (b), respectively. As can be seen in Fig. 8 (a), mode 2 is near 1 at 1.22 GHz, mode 3 and 4 are near 1 at around 1.6 GHz, suggesting resonances at 1.22 GHz and 1.6 GHz, which can be verified by the reflection coefficient of the proposed antenna (see Fig. 5 (a)). In addition, as stated earlier, for

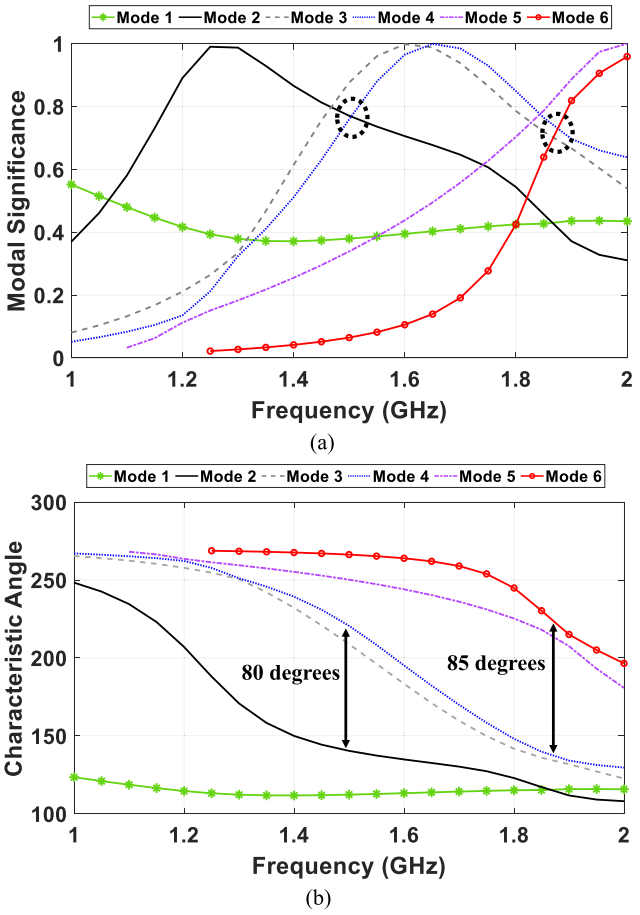

FIGURE 8. Characteristic mode analysis of the proposed antenna, (a) modal significance (b) characteristic angle (CA unit is in degree).

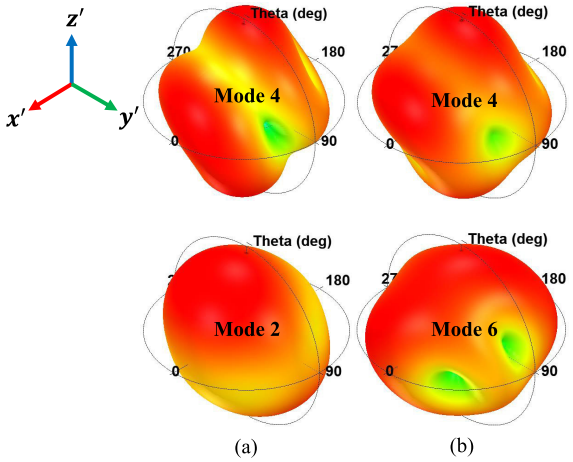

FIGURE 9. Far-field radiation patterns of the different modes of proposed antenna at two different frequencies, (a) 1.5 GHz (b) 1.85 GHz.

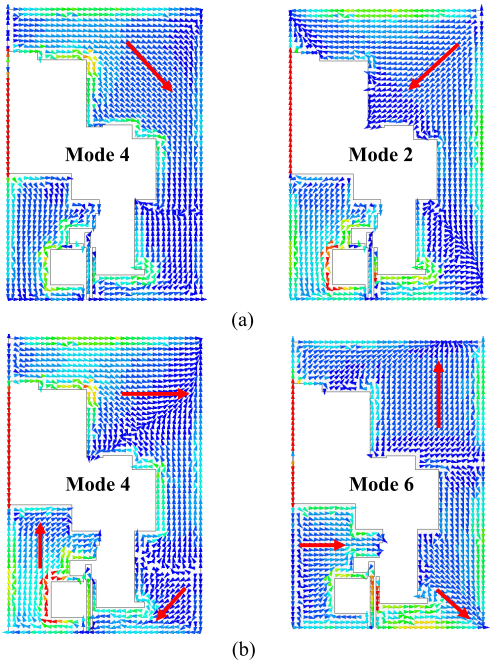

FIGURE 10. Surface currents of different modes of Ant4 at two different frequencies, (a) 1.5 GHz (b) 1.85 GHz.

having a circular polarization, two orthogonal modes should meet four requirements. It should be noticed that any pairs of modes which have the mentioned four requirements can help produce CP. Since AR<3dB is desired here, meeting the requirements with approximation can also be acceptable. The first requirement is to have two modes with equal MS value. Therefore, we should look for the frequencies in which two modes have equal values. For this, 1.5 GHz, and 1.85 GHz are chosen as an example. Secondly, the CAs should have around 90 degrees of phase delay. As shown in Fig. 8 (b), the CA of modes 2 and 4 have 80° phase difference which is capable of producing CP. Also, at 1.85 GHz, the phase difference between modes 4 and 6 is about 85°, all making the antenna potential of producing circular polarization. Thirdly, the directivity of each two orthogonal mode should be the same in the desired angle. In Fig. 9, far-field radiation patterns of different desired modes at different frequencies are depicted. All far-field patterns show directivities maximum at the desired angle of around $\theta' = 0$. Finally, the surface currents for the modes at different frequencies are demonstrated in Fig. 10, showing the orthogonality of each pair of modes at the desired frequency. Since the only difference between Ant4 and the proposed antenna geometries is in their transparency and applied mesh grid, the surface current of Ant4 is displayed instead of the proposed antenna. It is worth mentioning that since the CMA is just performed for the PEC radiator without any substrate and feeding, there might be some shifts in the desired frequencies, as can be seen in the CMA results.

IV. ANTENNA ANALYSIS AND TRANSPARENT REFLECTOR

A. CP MECHANISM

The CP mechanism of the proposed antenna is investigated by plotting the electric fields distribution of the antenna at four different time instants at GPS L2 center frequency band (1.227 GHz) as an example. It is worth mentioning that

although the process of circular polarization is investigated in CMA section, this section shows the final CP mechanism of the proposed antenna. As can be seen in Fig. 11, the field distribution at the middle section of the antenna is rotating as the time passes. The counter-clockwise rotation of the fields result in an RHCP wave radiation of the antenna. Also, the fields at the lower section of the antenna have notable contribution for producing circular polarization. As can be seen, the rotation of the lower section fields are the same as middle section in terms of the summation of field vectors pointing and being counter-clockwise in time propagation. The way that the electric fields distribution is observed has been shown in Fig. 11 (e).

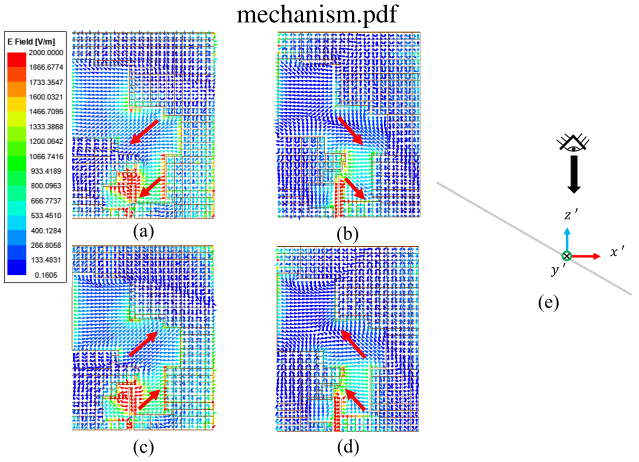

FIGURE 11. Electric fields distribution of the proposed antenna at four different time instants at GPS L2 center frequency (1.227 GHz), (a) 0° (b) 90° (c) 180°, (d) 270° (e) the way proposed antenna is observed for the electric fields distribution.

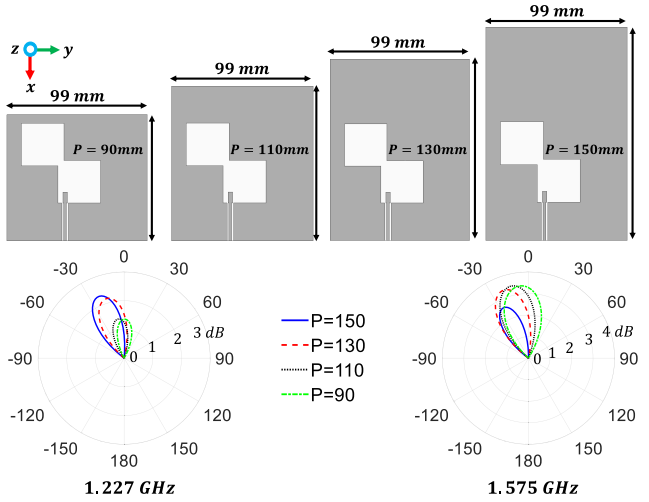

FIGURE 12. RHCP beam direction of the diagonal-slot antenna for different values of "*P*" in the primary coordinate system at $\phi = 0°$ for two different GPS frequency bands.

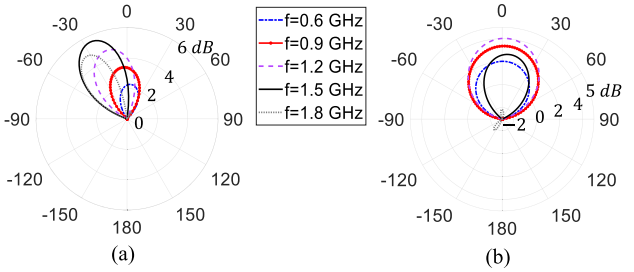

FIGURE 13. RHCP beam direction of the diagonal-slot antenna for different frequencies in the primary coordinate system at two different planes, (a) $\phi = 0°$ (b) $\phi = 90°$.

B. ANTENNA BEAM

To have a better observation of beam tilting, an antenna having two diagonal slots is investigated for observing the beam directions, shown in Fig. 12. This antenna is similar to Ant2, with some differences in the dimension of the slots and the overall length. The initial length of this antenna is 90 mm and increases to 150 mm (same length of Ant2). As shown in Fig. 12, by increasing the length of the antenna from upper side, the maximum beam direction of the antenna alters from $\theta = 0°$ to $\theta = 25°$ at 1.227 GHz, and from $\theta = 5°$ to about $\theta = 30°$ at 1.575 GHz at $\phi = 0°$ in the primary coordinate system. Therefore, an increase in the length of the antenna causes an increase in the tilted angle of the antenna in the desired plane and frequencies. In other words, for having an antenna with a tilted beam rather than 30°, the length of the antenna can be determined first. Then, other optimizations for obtaining circular polarization can be done.

As an another investigation, the RHCP beam directions of the proposed antenna for different frequencies in the primary coordinate system are demonstrated in Fig. 13. Increasing the operation frequency from 0.6 GHz to 1.8 GHz results in maximum beam directions from $\theta = 0°$ to around $\theta = 30°$ at the desired plane of $\phi = 0°$, while no sensible change can be observed at $\phi = 90°$. This shows that by increasing the length of the antenna in one direction, the beam of the antenna mostly steers in that specific direction, not the perpendicular directions. Moreover, the direction of the beam is almost constant in each GNSS channel bandwidth (for example, the beam direction is almost constant in GPS L2 band, from the beginning which is 1215 MHz, to the end which is 1239 MHz). Hence, by choosing the desired length and performing optimization, the antenna can be used on a surface with an inclination angle rather than 30°.

C. PARAMETRIC STUDY

The variation of two parameters of "L" and "W" and the simulation results of reflection coefficient and axial ratio against frequency are shown in Fig. 14 and Fig. 15. The results are obtained for Ant4 since it is very close to the proposed antenna in terms of simulation results. Moreover, it is easier to do the parametric study for Ant4 instead of the proposed antenna since changing the parameters of proposed antenna needs some modification in terms of mesh elements. Hence, it is preferred to carry out the study on Ant4.

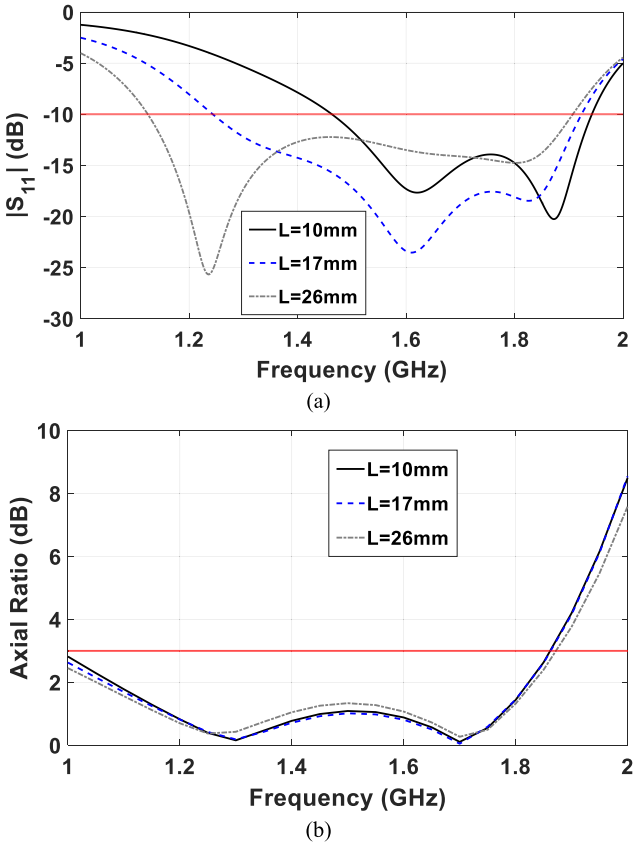

FIGURE 14. Simulation of Ant4 for different values of "*L*", (a) reflection coefficient (b) axial ratio.

Fig. 14 shows the variation of "L" and the corresponding results in terms of S_{11} and axial ratio. As discussed in sections II and III, Ant3 has a wide 3-dB axial ratio bandwidth, whereas the reflection coefficient shows that the antenna is not matched to a 50 Ω input feedline. Therefore, some slots are added to Ant3 to alter the effective electrical length of main radiator slots in the antenna structure and improve the reflection coefficient while keeping the 3-dB axial ratio bandwidth unchanged. In order to match a circuit to a certain transmission line with a certain characteristic impedance, from the theory, introducing a matching circuit at the beginning of the circuit would be one possible solution. In this case, the capacitive and inductive effects created by the matching circuit can improve the impedance bandwidth. One of the slots which plays the key role for 10-dB impedance bandwidth improvement is the slot with the length of "L". By adding the slot, it produces some capacitive and inductive effects which can alter the input impedance seen from the input of the antenna. By changing the length of the slot, the capacitive and inductive effects change and result in a change in the input impedance of the antenna, finally causing a change in the impedance bandwidth. As can be seen in Fig. 14 (a), by increasing the length of the slot, the impedance bandwidth becomes wider by shifting the lower end to lower frequencies, keeping the higher end almost unchanged. The axial ratio of the antenna however does not alter in the desired frequency band (see Fig. 14 (b)). Another important parameter is the width of the larger slot ("W"). As shown in previous section (CP mechanism), the electric fields distribution at the slots form a circular polarization. This means that by changing the size of main slots, the axial ratio value can be different. In Fig. 15, the reflection coefficient and axial ratio of Ant4 for different values of "W" are shown. This parameter has a significant impact on the upper end of the axial ratio bandwidth, while the lower end does not change much. By decreasing the value of "W", the axial ratio bandwidth becomes wider since the higher end of the bandwidth shift toward upper frequencies.

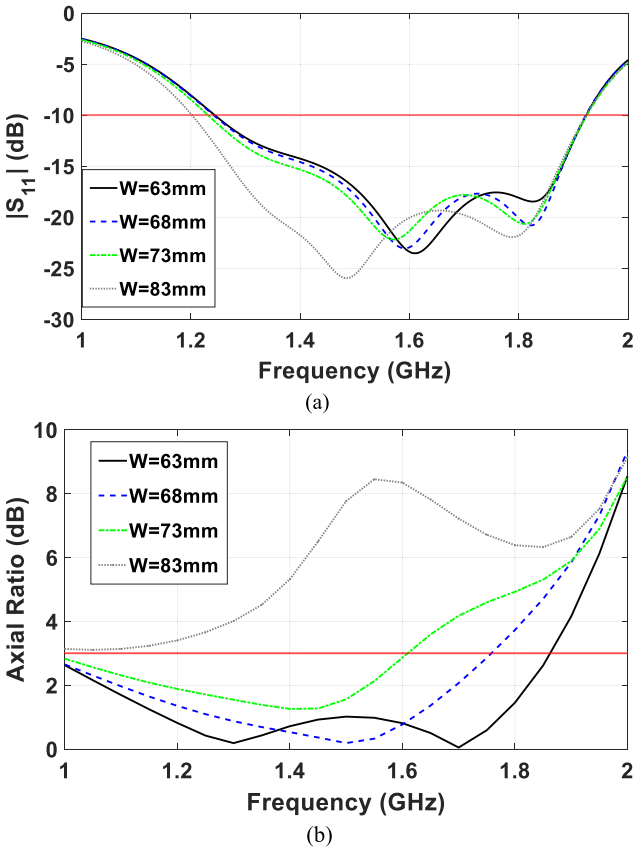

FIGURE 15. Simulation of Ant4 for different values of "*W*", (a) reflection coefficient (b) axial ratio.

Additionally, the effects of different scales of the proposed antenna (in both x- and y-directions with the same values) on the tilted angle in elevation plane are investigated. As shown in Fig. 16, by scaling the size of the antenna from the scale factors of $S = 0.8$ to $S = 1.1$, the tilted angle alters from $\theta = 17°$ to $\theta = 33°$ in the primary coordinate system. Here, scaling the antenna means that the dimensions of antenna including all its slots and strips are scaled with a constant value in both x- and y-directions. For instance, scale factor of 1.1 means that all the dimensions of the proposed antenna are multiplied by 1.1 in both x- and y-directions, and the scale factor of $S = 1$ is the proposed antenna, since scaling with

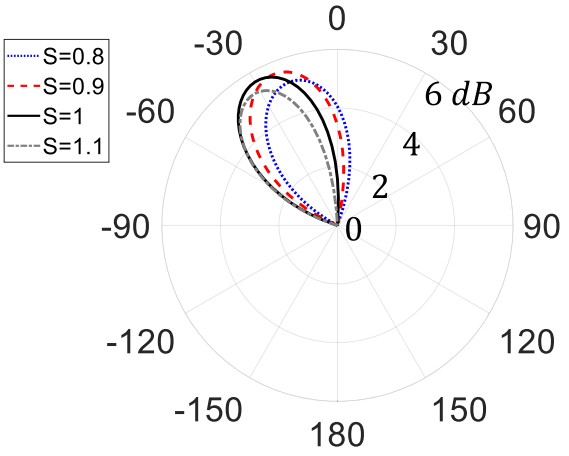

FIGURE 16. RHCP radiation patterns of the proposed antenna for different scale factors in the primary coordinate system at 1.575 GHz at $\phi = 0$.

a constant value of "1" does not change any dimensions. This behaviour is beneficial when the inclination angle of the surface (windshield here) is not exactly 30°. Therefore, by changing the scale factor parameter and performing optimization, the antenna can be used on a surface with an inclination angle rather than 30°. The RHCP radiation patterns of the proposed antenna for different scale factors in the primary coordinate system at 1.575 GHz for $\phi = 0$ plane are depicted in Fig. 16.

D. TRANSPARENT REFLECTOR

In GNSS (and especially GPS) applications, one of the key factors for having a better performance of the system is a high FBR, defined as the ratio of maximum RHCP and left hand circular polarization (LHCP) gain, while occurring at $\theta = 0°$ and $\theta = 180°$, respectively. However, in this work, since the beam of the antenna is tilted for around 30 degrees, the maximum RHCP gain occurs at around $\theta = 30°$, whereas maximum LHCP gain is at $\theta = 180° - 30° = 150°$, at the initial coordinate system. In the new coordinate system, however, this changes to $\theta' = 0$ and $\theta' = 180° - (2 \times 30°) = 120°$ for RHCP and LHCP maximum gains, respectively. Consequently, the terms "FBR" and "maximum RHCP and LHCP ratio" may be used interchangeably throughout the paper.

One of the common techniques for improving the FBR is to place a reflector below the antenna in a certain distance depended on the frequency of operation. Another important parameter is the size of the reflector which can determine the amount of FBR. The trade-off between the size of the reflector and FBR has always been a challenge. In this work, the target is to establish a balance between the size of the reflector and the FBR. Furthermore, since the proposed antenna is going to be mounted on the windshield, the reflector can be placed on the dashboard or glove compartment of the vehicle, fulfilling the required distance between the antenna and reflector. This will necessitate the need of the transparent reflector, instead of an opaque one.

Taking all above-mentioned information into consideration, a transparent small-size reflector with the dimensions of 100 × 100 mm^2 is designed with the usage of mesh grid in order to increase the transparency. The designed reflector is shown in Fig. 17 (a), and one mesh element is depicted in Fig. 17 (b). As discussed before, the transparency of reflector depends on the width of each trace "(n)" and length of the mesh element "(m)". Here, by setting $m = 5.4$ and $n = 0.1$ mm, the calculated transparency using Eqn 1 is about 95%. Afterwards, the reflector is put under the antenna with a distance of 85 mm from the center (or 48 mm from the lower edge) of the antenna. The isometric and side view of the final placements are illustrated in Fig. 17 (c) and (d), respectively. All simulation and measurement results are discussed in more details in the next section.

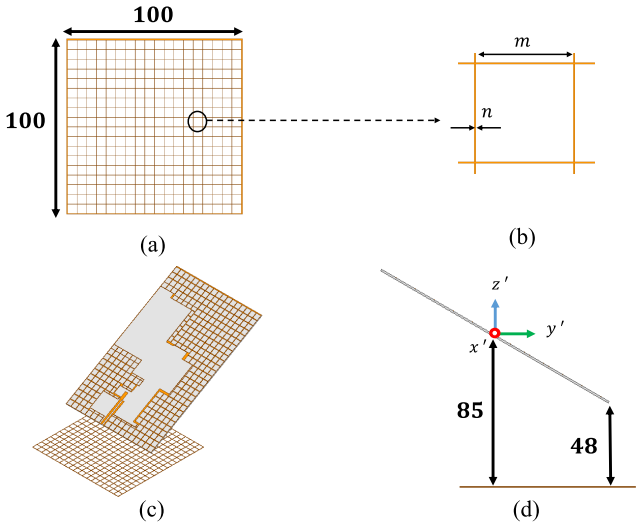

FIGURE 17. Transparent reflector and the way it is placed under the proposed antenna, (a) transparent reflector using mesh grid (b) one mesh element (c) isometric view of the reflector under the antenna (d) side view of the reflector and antenna (units in mm).

V. FABRICATION OF PROTOTYPES AND DISCUSSION OF SIMULATION AND MEASUREMENT RESULTS

A. FABRICATION PROCESS

The antenna is fabricated by the 3D printing method. Other methods like pasting the antenna made by transparent flexible printed circuit board (FPCB) on the glass (made by PET films) also could be considered [24]. The fabrication process of the proposed antenna is done in two major steps. In the first step, the antenna is fabricated by printing conductive silver ink on two equal-size Corning® Boro-Aluminosilicate glass with dielectric constant of $\epsilon_r = 5.5$ and thickness of 1 mm, with a precision of 0.1 mm for mesh traces. Afterwards, the two halves are connected and integrated with each other, forming the final prototype. Noteworthy, if the silver blackens, the reflection from the antenna will be less that will improve transparency. For resemblance of windshield and its

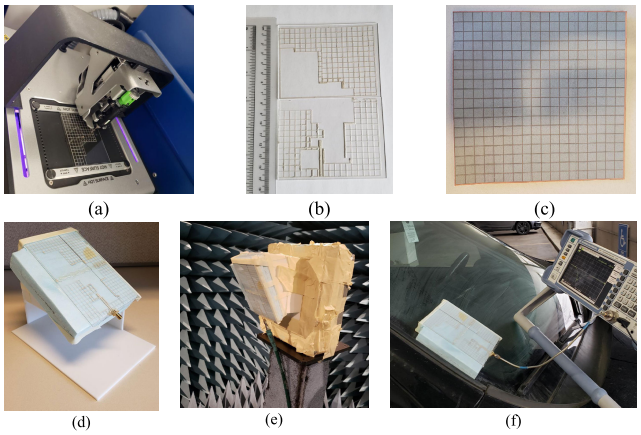

FIGURE 18. Fabrication and measurement of the proposed antenna, (a) fabrication process (b) proposed antenna before integration (c) fabricated transparent reflector (d) fabricated antenna on the inclined stage (e) measurement of the fabricated antenna in anechoic chamber (f) measurement of reflection coefficient of the proposed antenna on the windshield of vehicle.

inclination angle, an inclined stage with an angle of 30° is fabricated using 3D printing. The material of stage is chosen to be very close to air, not to have a significant impact on the measurement results. Also, the stage is designed in a way to be capable of holding the reflector with the desired distance under the antenna. The measurements are carried out in anechoic chamber for two states of with and without the reflector. Finally, the reflection coefficient of the antenna while placed on the windshield of a vehicle is obtained. Fig. 18 illustrates all the above-mentioned steps. It is worth mentioning that the antenna can be printed by the same technology of high precision printing technique on the windshields of the vehicles.

B. RESULTS AND DISCUSSION

The simulation and measurement results of the proposed antenna in terms of reflection coefficient and axial ratio are depicted in Fig. 19 (a) and (b), respectively. As shown, the reflection coefficient is measured in two different states of normal (when it is measured in the lab) and on the windshield of a vehicle. The results show a very close agreement between the three plots, having a wide 10-dB impedance bandwidth of 40.8% (1.13 - 1.71 GHz). The axial ratio simulation and measurement results are also plotted in Fig. 19 (b), showing a 3-dB axial ratio bandwidth of 52% (1.04 - 1.77 GHz) in the simulation and 47.4% (1.06 - 1.72 GHz) in the measurements. Both the impedance and axial ratio bandwidths cover the entire GNSS bands, starting from 1.16 GHz to 1.61 GHz. Noteworthy, the axial ratio measurement is done in the new coordinate system.

The normalized radiation patterns of the antenna while it is mounted on the inclined stage are demonstrated in Fig. 20 and 21, with and without the presence of the reflector, respectively. The patterns in Fig. 20 are plotted at GPS L2 and L1 center frequencies at $\phi = 0°$ and $\phi = 90°$ planes, in the new coordinate system. The maximum RHCP gain

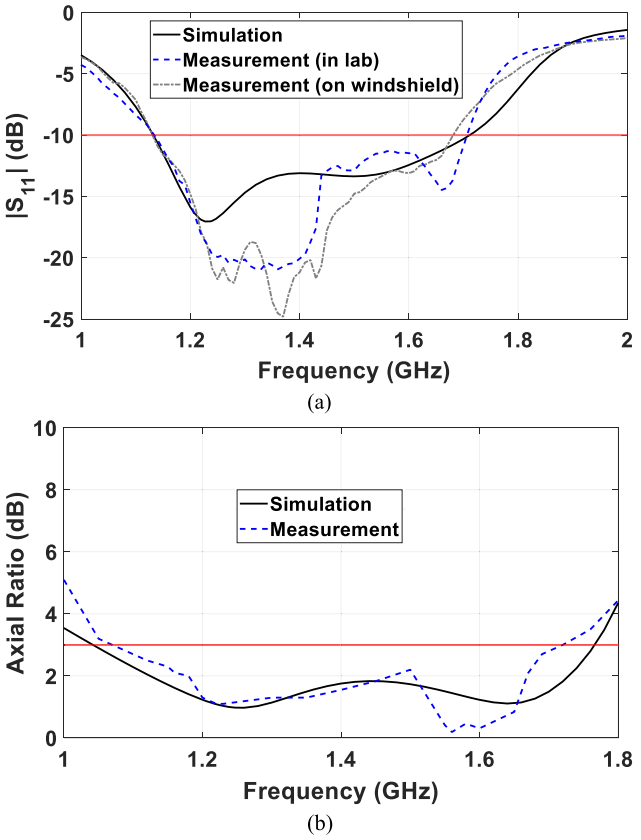

FIGURE 19. Simulation and measurement results of the proposed antenna, (a) reflection coefficient (b) axial ratio at $\theta' = 0$ and $\phi = 0$ (while mounted on the inclined stage).

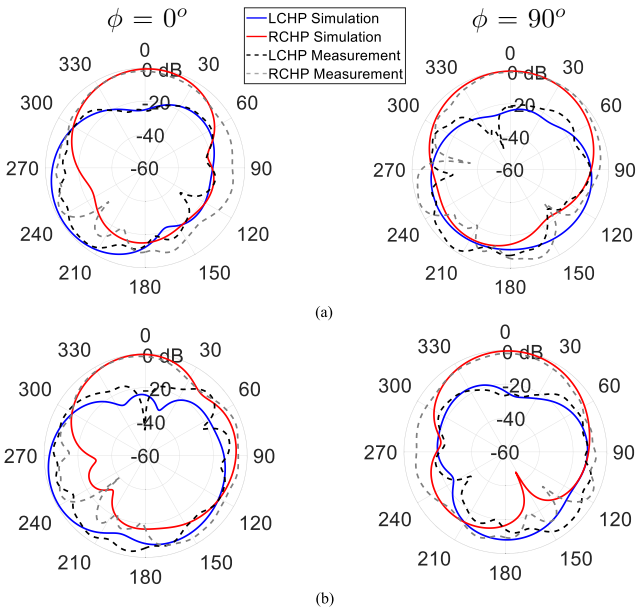

FIGURE 20. Normalized radiation pattern of the proposed antenna while placed on the inclined stage in the new coordinate system at two different frequencies, (a) 1.227 GHz (b) 1.575 GHz.

occurs at $\theta' = 0$, with an RHCP gain of 4.87 dBic and 5 dBic at GPS L2 and L1 bands, respectively. Also, the RHCP maximum gain while the reflector is put below the antenna is

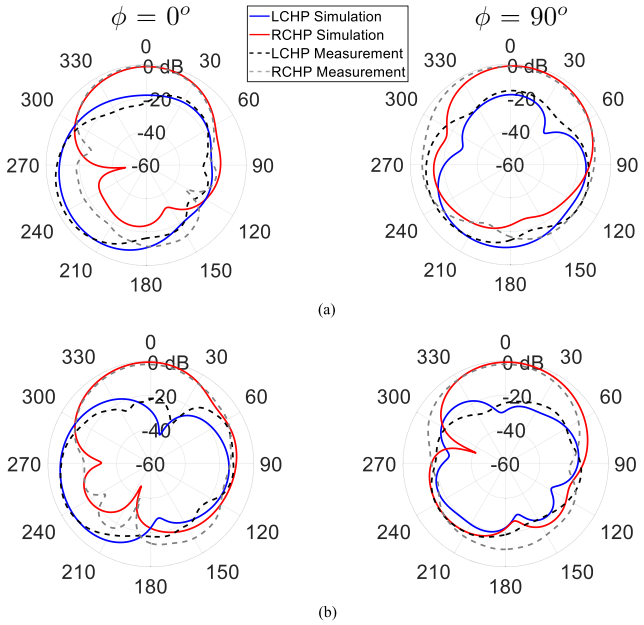

FIGURE 21. Normalized radiation pattern of the proposed antenna while placed on the inclined stage with the reflector below the antenna, in the new coordinate system at two different frequencies, (a) 1.227 GHz (b) 1.575 GHz.

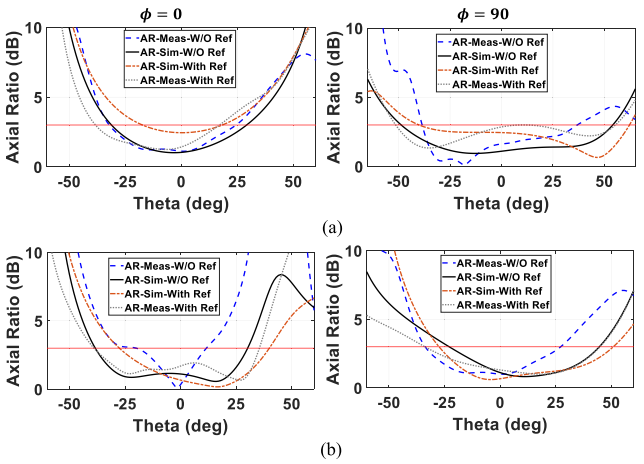

FIGURE 22. AR beamwidth of the proposed antenna in two different scenarios of with and without reflector at two different planes of $\phi = 0$ and $\phi = 90$, (a) 1.227 GHz (b) 1.575 GHz.

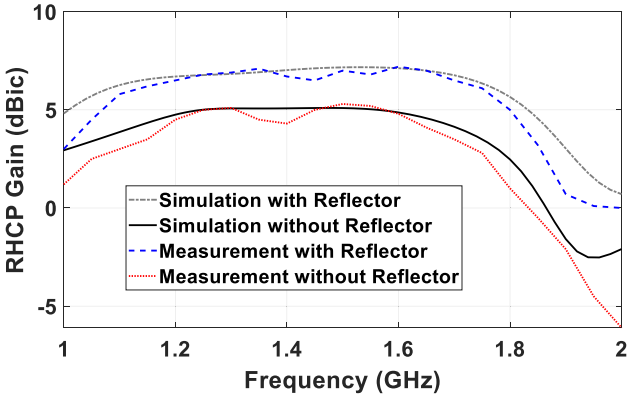

FIGURE 23. Simulation and measurement results of RHCP gain of the proposed antenna with and without the reflector at $\theta' = 0$ and $\phi = 0$.

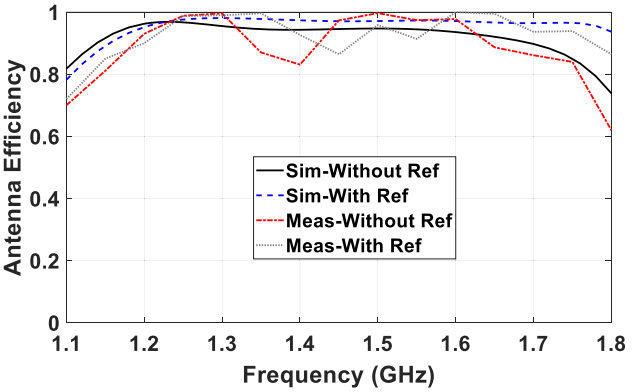

FIGURE 24. The efficiency of the proposed antenna for both scenarios of with and without reflector.

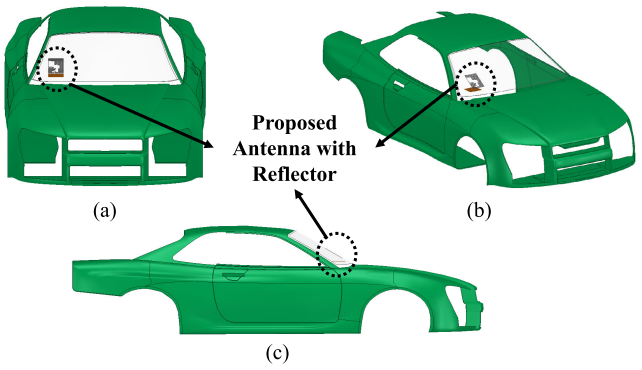

FIGURE 25. Proposed antenna with the reflector on a car model for re-simulation, (a) front view (b) isometric view (c) side view.

about 6.75 dBic at GPS L2, and 7.1 dBic at GPS L1 center frequencies, respectively. The measured half power beam width (HPBW) is more than 60°. Moreover, Fig. 21 shows the radiation patterns of antenna with the reflector placed on the stage. Both the simulation and measurement results show an improvement of FBR for at least 5 dB, which is desirable since the reflector size is small compared to the size of the antenna. The AR beamwidths of the proposed antenna in two different scenarios of with and without reflector at 1.227 GHz and 1.575 GHz are depicted in Fig. 22. The results show a minimum and maximum of 34° and 107° of AR beamwidths, occurring at 1.575 GHz at $\phi = 0°$, and 1.227 GHz at $\phi = 90°$, respectively. Furthermore, RHCP gain results at $\theta' = 0$ and $\phi = 0°$ against frequency with and without the reflector are depicted in Fig. 23. The measured maximum RHCP gain is about 7.1 dBic occurring at 1.35 GHz and 5.3 dBic at 1.5 GHz for the scenarios of with and without reflector, having a 3-dB gain bandwidth of 56.3% (1.02 - 1.82 GHz) and 54.2% (1.02 - 1.78 GHz), respectively. The results show that the reflector not only increases the FBR,

TABLE 1. Comparison between several single, dual, and wide band antennas in literature and the proposed antenna.

Design	Size (λ_0^2)	Type	IBW (Lower,Upper) (%)	ARBW (Lower,Upper) (%)	Tilted angle (deg)	Transparency (%)
[8]	0.74 × 0.74	Single-band	4	10.7	49	NA
[25]	0.41 × 0.41	Wideband	42	2.1 , 2	Not Tilted	Not Transparent
[26]	0.57 × 0.57	Dual-band	16.9 , 11.4	19.2 , 18	Not Tilted	Not Transparent
[27]	0.41 × 0.41	Dual-band	3.7, 1.2	0.9 , 0.6	Not Tilted	Not Transparent
[28]	0.53 × 0.53	Wideband	40.57	6.56 , 7.74	Not Tilted	Not Transparent
[29]	0.28 × 0.28	Single-band	3.2	1.7	Not Tilted	Not Transparent
[30]	4.52 (2.4 Diameter)	Wideband	35	Not CP	Not Tilted	100
[31]	0.26 × 0.19	Wideband	20	25	Not Tilted	Not Transparent
[32]	0.988 ×0.52	Wideband	40	6.19	30	Not Transparent
[33]	0.48 × 0.175	Wideband	26 *	Not CP	Not Tilted	>70
[34]	0.62 (0.89 Diameter)	Wideband	42	Not CP	Not Tilted	100
[35]	0.49 ×0.49	Single-band	7	Not CP	Not Tilted	94
[36]	0.88 ×0.88	Wideband	19	Not CP	Not Tilted	70
[37]	0.4 ×0.4	Single-band	4	Not CP	Not Tilted	60
This work	0.56 × 0.37	Wideband	40.8	47.4	30	95

λ_0 is the free space wavelength at the lowest operating frequency.
* The 10-dB IBW is obtained from the figures in the paper.

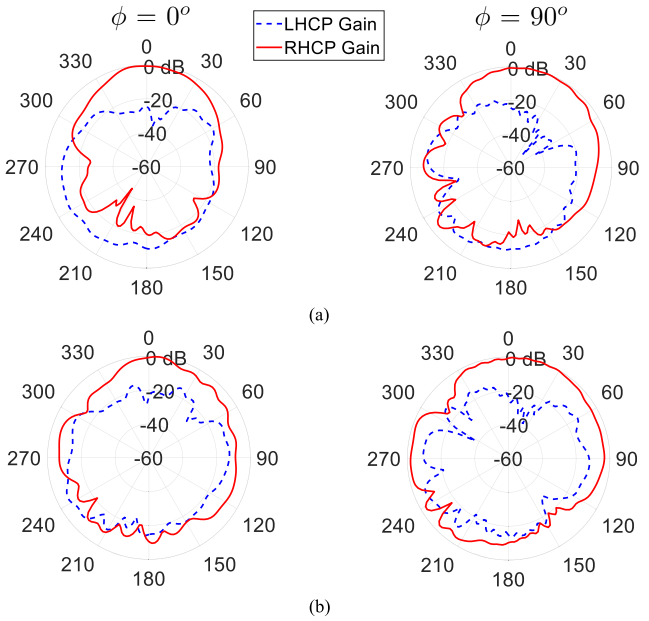

FIGURE 26. Simulated normalized radiation pattern of the proposed antenna on the car model at two different frequencies with the reflector under the antenna, (a) 1.227 GHz (b) 1.575 GHz.

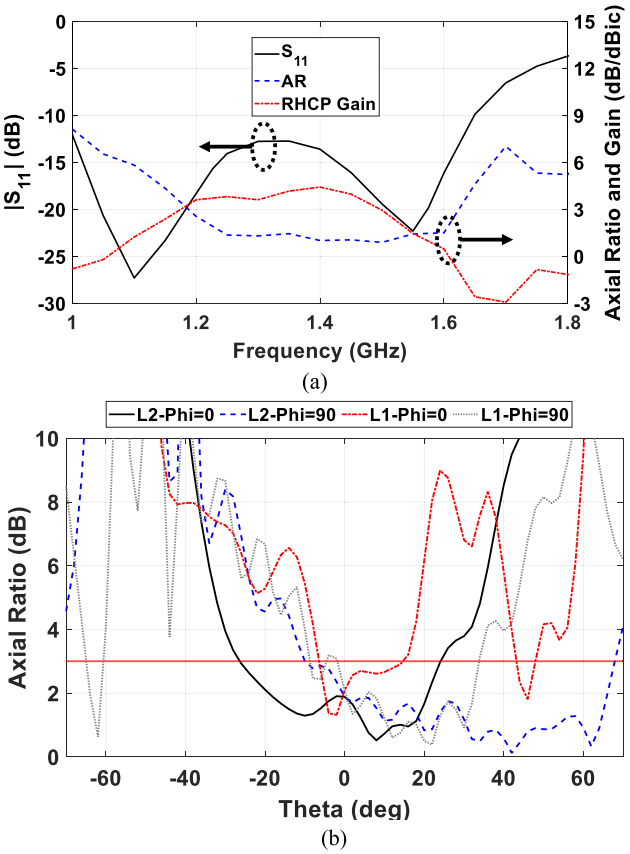

FIGURE 27. Simulated results of the proposed antenna when the car model is included, (a) reflection coefficient, AR, and RHCP gain at $\theta' = 0$ and $\phi = 0$, (b) AR beamwidths for two different planes of $\phi = 0$ and $\phi = 90$ at 1.227 GHz and 1.575 GHz.

but also improves the RHCP gain. The efficiency of the proposed antenna in both scenarios are demonstrated in Fig. 24. As can be observed, the efficiency of the antenna is more than 80 % in the desired bandwidth.

C. COMPARISON WITH PREVIOUS WORKS IN LITERATURE

Table 1 shows the comparison of the proposed antenna with other similar previous works in literature. As can be seen, there are no other previous works having all the characteristics of being wideband, CP, tilted beam, and transparent at the same time. As discussed earlier, designing an antenna on a single-layer having all the characteristics together and adding a transparent reflector under the antenna on the dashboard or glove compartment of the car, is the main novelty of this work.

D. RESULTS ON A CAR MODEL

To see the effects of different parts of the vehicle (such as the roof, hood, doors and so forth) on the radiation patterns,

the proposed antenna with the reflector are put on the glove compartment of a metallic car model, shown in Fig. 25. For simplicity, PEC is chosen as the material of the car model. The radiation patterns are represented in Fig. 26 for GPS L2 and L1 center frequencies at two different planes. Same as the previous results, the new coordinate system is chosen and, consequently, the maximum RHCP gain is expected to occur at $\theta' = 0$, with an acceptable FBR. The results in Fig. 26 verify the acceptable performance of the antenna while it is mounted on the windshield. Furthermore, the simulation results of reflection coefficient, axial ratio, and RHCP gain versus frequency at $\theta' = 0$ and $\phi = 0$ are demonstrated in Fig. 27 (a), while the axial ratio beamwidths of the proposed antenna when the car model is included are presented in Fig. 27 (b) for two different planes of $\phi = 0$ and $\phi = 90$ at two different frequencies of GPS L2 and L1 bands. The results show a wide 10-dB impedance bandwidth of 49% (1 - 1.65 GHz) with a wide 3-dB axial ratio bandwidth of 30.6% (1.19 - 1.62 GHz). The maximum RHCP gain with the value of 4.4 dBic also occurs at 1.4 GHz. Moreover, the AR beamwidths represented in Fig. 27 (b) show a minimum beamwidth of 22° at 1.575 GHz and a maximum beamwidth of 78° at 1.227 GHz. In summary, the results of the proposed antenna on the car model show an acceptable performance for the desired application. Noteworthy, by adding the car model, the time of the simulation increases as the dimension of the whole region increases very much compared with the single antenna. Here, the simulation has taken about 50 minutes having multiple cores with parallel analysis.

VI. CONCLUSION

In this paper, a single-layer wideband CPW-fed transparent CP antenna with tilted beam is proposed. The antenna has a wideband 10-dB impedance bandwidth of 40.8% (1.13 - 1.71 GHz) and a wideband 3-dB axial ratio bandwidth of 47.4% (1.06 - 1.72 GHz) and a 3-dB gain bandwidth of 54% (1.02 - 1.78 GHz) are obtained in the measurements, covering the whole GNSS frequency bands. The RHCP gain of the antenna at $\theta' = 0$ and $\phi = 0°$ is about 6.75 and 7.1 dBic at GPS L2 and L1 bands respectively, in the presence of the reflector. The antenna is fabricated on Corning® Boro-Aluminosilicate glass with $\epsilon_r = 5.5$ and thickness of 1 mm. Mesh grid is used for the conductive layer of the antenna, instead of a full layer. The transparency of the antenna is about 95%. The operation of antenna is investigated with characteristic mode analysis. Furthermore, to increase the FBR and RHCP gain of the antenna, a small-size transparent reflector is designed and placed under the antenna with a certain distance. The radiation patterns show a tilted beam antenna with an acceptable performance in terms of reflection coefficient, axial ratio, RHCP gain, FBR, and so on. In the final step, the antenna is re-simulated on a car model to see the effects of different parts of a car on the radiation patterns. The proposed antenna is suitable for inclined surfaces and also for GNSS/GPS applications, such as location tracking of the vehicles. Comparing to the previous works in literature, no other such antennas being wideband, CP, transparent, and tilted beam were proposed.

ACKNOWLEDGMENT

The authors would like to acknowledge that this project is supported by NovAtel Inc., in fabrications, CMC Microsystems for providing software, and Alberta Innovate (AI).

REFERENCES

[1] R. Xu, J.-Y. Li, J.-J. Yang, K. Wei, and Y.-X. Qi, "A design of U-shaped slot antenna with broadband dual circularly polarized radiation," *IEEE Trans. Antennas Propag.*, vol. 65, no. 6, pp. 3217–3220, Jun. 2017.

[2] W.-M. Li, B. Liu, and H.-W. Zhao, "The U-shaped structure in dual-band circularly polarized slot antenna design," *IEEE Antennas Wireless Propag. Lett.*, vol. 13, pp. 447–450, 2014.

[3] Z. Wu, M. Yao, H. Ma, W. Jia, and F. Tian, "Low-cost antenna attitude estimation by fusing inertial sensing and two-antenna GPS for vehicle-mounted satcom-on-the-move," *IEEE Trans. Veh. Technol.*, vol. 62, no. 3, pp. 1084–1096, Mar. 2013.

[4] N. Nadarajah, P. J. G. Teunissen, and N. Raziq, "Instantaneous GPS–Galileo attitude determination: Single-frequency performance in satellite-deprived environments," *IEEE Trans. Veh. Technol.*, vol. 62, no. 7, pp. 2963–2976, Sep. 2013.

[5] A. Gharaati, M. S. Ghaffarian, H. Saghlatoon, M. Behdani, and R. Mirzavand, "A low-profile wideband circularly polarized CPW slot antenna," *AEU-Int. J. Electron. Commun.*, vol. 129, Feb. 2021, Art. no. 153534.

[6] M. S. Ghaffarian, G. Moradi, and P. Mousavi, "Wide-b-and circularly polarised slot antenna by using artificial transmission line," *IET Microw., Antennas Propag.*, vol. 11, no. 5, pp. 672–679, 2016.

[7] A. Gharaati, S. Ghaffarian, R. Mirzavand, and P. Mousavi, "Transparent circularly-polarized antenna with tilted beam for vehicular platforms," in *Proc. IEEE Int. Symp. Antennas Propag. North Amer. Radio Sci. Meeting*, Jul. 2020, pp. 117–118.

[8] H. Zhou, A. Pal, A. Mehta, D. Mirshekar-Syahkal, and H. Nakano, "A four-arm circularly polarized high-gain high-tilt beam curl antenna for beam steering applications," *IEEE Antennas Wireless Propag. Lett.*, vol. 17, no. 6, pp. 1034–1038, Apr. 2018.

[9] W. D. Ake, M. Pour, and A. Mehrabani, "Asymmetric half-bowtie antennas with tilted beam patterns," *IEEE Trans. Antennas Propag.*, vol. 67, no. 2, pp. 738–744, Feb. 2018.

[10] A. Mehmood, O. H. Karabey, and R. Jakoby, "Dielectric resonator antenna with tilted beam," *IEEE Antennas Wireless Propag. Lett.*, vol. 16, pp. 1119–1122, 2017.

[11] R. B. Green, M. Guzman, N. Izyumskaya, B. Ullah, S. Hia, J. Pitchford, R. Timsina, V. Avrutin, U. Ozgur, H. Morkoc, N. Dhar, and E. Topsakal, "Optically transparent antennas and filters: A smart city concept to alleviate infrastructure and network capacity challenges," *IEEE Antennas Propag. Mag.*, vol. 61, no. 3, pp. 37–47, Jun. 2019.

[12] S. H. Kang and C. W. Jung, "Transparent patch antenna using metal mesh," *IEEE Trans. Antennas Propag.*, vol. 66, no. 4, pp. 2095–2100, Apr. 2018.

[13] F. Colombel, X. Castel, M. Himdi, G. Legeay, S. Vigneron, and E. M. Cruz, "Ultrathin metal layer, ITO film and ITO/Cu/ITO multilayer towards transparent antenna," *IET Sci., Meas. Technol.*, vol. 3, no. 3, pp. 229–234, May 2009.

[14] M. Kashanianfard and K. Sarabandi, "Vehicular optically transparent UHF antenna for terrestrial communication," *IEEE Trans. Antennas Propag.*, vol. 65, no. 8, pp. 3942–3949, Aug. 2017.

[15] J. R. Saberin and C. Furse, "Challenges with optically transparent patch antennas," *IEEE Antennas Propag. Mag.*, vol. 54, no. 3, pp. 10–16, Jun. 2012.

[16] T. Yasin, R. Baktur, and C. Furse, "A study on the efficiency of transparent patch antennas designed from conductive oxide films," in *Proc. IEEE Int. Symp. Antennas Propag. (APSURSI)*, Jul. 2011, pp. 3085–3087.

[17] R. J. Garbacz and R. Turpin, "A generalized expansion for radiated and scattered fields," *IEEE Trans. Antennas Propag.*, vol. AP-19, no. 3, pp. 348–358, May 1971.

[18] R. F. Harrington and J. R. Mautz, "Theory of characteristic modes for conducting bodies," *IEEE Trans. Antennas Propag.*, vol. AP-19, no. 5, pp. 622–628, Sep. 1971.

[19] Y. Chen and C.-F. Wang, *Characteristic Modes: Theory and Applications in Antenna Engineering*. Hoboken, NJ, USA: Wiley, 2015.
[20] M. Han and W. Dou, "Compact clock-shaped broadband circularly polarized antenna based on characteristic mode analysis," *IEEE Access*, vol. 7, pp. 159952–159959, 2019.
[21] R. Xu, S. Gao, J. Liu, J.-Y. Li, Q. Luo, W. Hu, L.-H. Wen, X.-X. Yang, and J. S. Sumantyo, "Analysis and design of ultrawideband circularly polarized antenna and array," *IEEE Trans. Antennas Propag.*, vol. 68, no. 12, pp. 7842–7853, Dec. 2020.
[22] H. H. Tran, N. Nguyen-Trong, and A. M. Abbosh, "Simple design procedure of a broadband circularly polarized slot monopole antenna assisted by characteristic mode analysis," *IEEE Access*, vol. 6, pp. 78386–78393, 2018.
[23] C. Zhao and C. F. Wang, "Characteristic mode design of wide band circularly polarized patch antenna consisting of H-shaped unit cells," *IEEE Access*, vol. 6, pp. 25292–25299, 2018.
[24] Y. Han, Z. Liu, C. Zhang, C. Mei, Q. Chen, K. Hu, and S. Yuan, "A flexible microstrip low-pass filter design using asymmetric Pi-shaped DGS," *IEEE Access*, vol. 7, pp. 49999–50006, 2019.
[25] C. Deng, Y. Li, Z. Zhang, G. Pan, and Z. Feng, "Dual-band circularly polarized rotated patch antenna with a parasitic circular patch loading," *IEEE Antennas Wireless Propag. Lett.*, vol. 12, pp. 492–495, 2013.
[26] M. Ramirez and J. Parron, "Concentric annular ring slot antenna for global navigation satellite systems," *IEEE Antennas Wireless Propag. Lett.*, vol. 11, pp. 705–707, 2012.
[27] W.-T. Hsieh, T.-H. Chang, and J.-F. Kiang, "Dual-band circularly polarized cavity-backed annular slot antenna for GPS receiver," *IEEE Trans. Antennas Propag.*, vol. 60, no. 4, pp. 2076–2080, Apr. 2012.
[28] S. Lee, Y. Yang, K.-Y. Lee, and K. C. Hwang, "Dual-band circularly polarized annular slot antenna with a lumped inductor for GPS application," *IEEE Trans. Antennas Propag.*, vol. 68, no. 12, pp. 8197–8202, Dec. 2020.
[29] J. Yuan, J. Zheng, and Z. D. Chen, "A compact meandered ring antenna loaded with parasitic patches and a slotted ground for global navigation satellite systems," *IEEE Trans. Antennas Propag.*, vol. 66, no. 12, pp. 6835–6843, Dec. 2018.
[30] J. Sun and K.-M. Luk, "A wideband low cost and optically transparent water patch antenna with omnidirectional conical beam radiation patterns," *IEEE Trans. Antennas Propag.*, vol. 65, no. 9, pp. 4478–4485, Sep. 2017.
[31] E. F. Sundarsingh and A. Harshavardhini, "A compact conformal windshield antenna for location tracking on vehicular platforms," *IEEE Trans. Veh. Technol.*, vol. 68, no. 4, pp. 4047–4050, Apr. 2019.
[32] W.-H. Zhang, W.-J. Lu, and K.-W. Tam, "Circularly polarized complementary antenna with tilted beam based on orthogonal dipoles," *IEEE Antennas Wireless Propag. Lett.*, vol. 17, no. 8, pp. 1406–1410, Aug. 2018.
[33] P. Duy Tung and C. W. Jung, "Optically transparent wideband dipole and patch external antennas using metal mesh for UHD TV applications," *IEEE Trans. Antennas Propag.*, vol. 68, no. 3, pp. 1907–1917, Mar. 2019.
[34] J. Sun and K.-M. Luk, "A compact-size wideband optically-transparent water patch antenna incorporating an annular water ring," *IEEE Access*, vol. 7, pp. 122964–122971, 2019.
[35] A. S. M. Sayem, R. B. V. B. Simorangkir, K. P. Esselle, R. M. Hashmi, and H. Liu, "A method to develop flexible robust optically transparent unidirectional antennas utilizing pure water, PDMS, and transparent conductive mesh," *IEEE Trans. Antennas Propag.*, vol. 68, no. 10, pp. 6943–6952, Oct. 2020.
[36] C. Ding, L. Liu, and K.-M. Luk, "An optically transparent dual-polarized stacked patch antenna with metal-mesh films," *IEEE Antennas Wireless Propag. Lett.*, vol. 18, no. 10, pp. 1981–1985, Oct. 2019.
[37] S. Hong, Y. Kim, and C. W. Jung, "Transparent microstrip patch antennas with multilayer and metal-mesh films," *IEEE Antennas Wireless Propag. Lett.*, vol. 16, pp. 772–775, 2016.

ALIREZA GHARAATI (Graduate Student Member, IEEE) received the B.Sc. degree in electrical engineering from the University of Tehran, Tehran, Iran, in 2018. He is currently pursuing the M.Sc. degree with the University of Alberta, Edmonton, AB, Canada. His current research interests include antenna and propagation, and RF/microwave circuits. He was a recipient of Honorable Mention from IEEE International Symposium on Antennas and Propagation and North American Radio Science, in 2020. He received the RGL Mousavi-Daneshmand Engineering Innovation Award, in 2020.

MOHAMMAD SAEID GHAFFARIAN (Member, IEEE) received the B.Sc. degree in telecommunication engineering from Ferdowsi University of Mashhad, Mashhad, Iran, in 2009, and the M.Sc. and Ph.D. degrees in electrical engineering from the Amirkabir University of Technology, Tehran, Iran, in 2011 and 2017, respectively. He is currently a Postdoctoral Fellow with the Intelligent Wireless Technology (IWT) Laboratory, University of Alberta, Edmonton, Canada. His research interests include small antennas, transparent antennas, phased array antennas, sensors and metamaterial. He received the Best M.Sc. Researcher Award in Telecommunications from the Amirkabir University of Technology, in 2011.

RASHID MIRZAVAND (Senior Member, IEEE) received the B.Sc. degree in electrical engineering from Isfahan University of Technology, in 2004, and the M.Sc. and Ph.D. degrees in electrical engineering from the Amirkabir University of Technology, in 2007 and 2011, respectively.

From 2012 to 2015, he was an Assistant Professor with the Amirkabir University of Technology. Since 2015, he has been the Principal Scientist and the Head of Research and is currently the Director of the Intelligent Wireless Technology Laboratory. He is also an Adjunct Professor with the University of Alberta. He is a Co-Founder of three companies from the University of Alberta. He is the coauthor of more than 170 papers published in refereed journals and conferences proceedings. His research interests include, but are not limited to, microwave/mm-wave circuits, sensors, measurement systems, and antennas. He received various awards, such as Best AUT M.Sc. Researcher 2007, Best AUT Ph.D. Researcher 2011, Best MICT National Researcher 2013, National Elite Foundation Young Professor Grant 2014, AITF Elite PDF 2015, Honorable CMC Industrial Collaboration 2017, TEC Edmonton Innovation 2019, CMC Industrial Collaboration 2021, and UofA Innovation 2021.